Supporting information for

Interfacial engineering with trivalent cation for efficient and stable inverted inorganic perovskite solar cells

Zezhang Wang[1], Tianfei Xu[1], Nan Li[1], Yali Liu [1], Kun Li[1], Zihao Fan[1], Jieke Tan[1], Dehong Chen[3], Shengzhong Liu[1,2,3,*], Wanchun Xiang[1,*]

[1]Key Laboratory of Applied Surface and Colloid Chemistry, Ministry of Education, Shaanxi Key Laboratory for Advanced Energy Devices, Shaanxi Engineering Lab for Advanced Energy Technology, School of Materials Science and Engineering, Shaanxi Normal University, Xi'an, 710119, China. wanchun.xiang@snnu.edu.cn

[2]Key Laboratory of Photoelectric Conversion and Utilization of Solar Energy, Dalian Institute of Chemical Physics, Chinese Academy of Sciences, Dalian, 116023, Liaoning, China. szliu@dicp.ac.cn

[3]Center of Materials Science and Optoelectronics Engineering, University of Chinese Academy of Sciences, Beijing, 100049, P. R. China

[4]College of Materials Science and Engineering, Qingdao University of Science & Technology, Qingdao, 266042, China

Experiment Section

Materials:

The F-doped tin oxide (FTO) glass was purchased from Suzhou Shangyang Technology. Dimethylamine-lead triiodide ($DMAPbI_3$, 99%), [2-(3,6-Dimethoxy-9H-carbazol-9-yl)ethyl] phosphonic acid (MeO-2PACz) and Li-bis-(trifluoromethanesulphonyl) imide (LiTFSI. 99%) were purchased from Xi'an e-Light New Material Co.,Ltd. Cesium iodide (CsI, 99.99%), lead bromide ($PbBr_2$, 99.99%) were purchased from Borun New Material Technology Ltd. Bathocuproine (BCP) was purchased from Thermo Fisher Scientific. 1-dodecyl-3-methylimidazolium bromide (DMIB), ytterbium (III) trifluoromethanesulfonate ($Yb(TFSI)_3$, 99.99%), sodium trifluoromethanesulfinate (NaTFSI, 98%), 4-tert-butylpyridine (tBP), chlorobenzene (CB, ≥99%) and N,N-dimethylformamide (DMF, ≥99.8%) were purchased from Sigma-Aldrich. 2,2',7,7'-Tetrakis [N,N-di(4-methoxyphenyl)amino]-9,9'-spirobifluorene (Spiro-OMeTAD, 99.8%), [6,6]-phenyl-C61-butyric acid methyl ester ($PC_{61}BM$) and NiO_x nanoparticles were purchased from Advanced Election Technology Co. Ltd. Dimethyl sulfoxide (DMSO, ≥99.9%), isopropanol (IPA, ≥99.7%) and ethyl acetate (EA) were purchased from Chinese National Pharmaceutical Group Corporation. Ytterbium (III) acetate ($Yb(AC)_3$), ytterbium (III) Acetylacetonate ($Yb(ACAC)_3$) were purchased from Shanghai Aladdin Biochemical Technology Co., Ltd.

Solution preparation:

MeO-2PACz was dissolved in IPA to prepare a solution to obtain self-assembly monolayer (SAM) solution (1 mg mL^{-1}). The 0.6 M perovskite precursor solution was prepared by mixing CsI, $DMAPbI_3$ and $PbBr_2$ (molar ratio = 3.0:2.8:0.2) in DMF and DMSO (volume ratio = 8:2). PCBM was dissolved in CB with a concentration of 20 mg mL^{-1}. Different amounts of $Yb(TFSI)_3$ were dissolved in EA (0.1, 0.3, 0.6, 1.0 mg mL^{-1}). NaTFSI was also dissolved in EA. The spiro-OMeTAD solution was prepared by dissolving 90 mg spiro-OMeTAD, 36 μL tBP and 22 μL LiTFSI (520 mg mL^{-1} in acetonitrile) in 1 mL CB. The above solutions were stirred for at least 6 h at room temperature. BCP was dissolved in IPA (1 mg mL^{-1}) in an ultrasonic bath for 12 h. All solutions

were filtered through a 0.45 μm syringe filter before use. NiO_x nanoparticles were dissolved in deionized water and the 10 mg mL^{-1} NiO_x aqueous solution was filtered by a 0.2 μm syringe filter.

Device fabrication:

FTO-glass substrate (2.5×2.5 cm^2, 15 Ω sq^{-1}) was sequentially cleaned with acetone, isopropanol and ethanol for 30 min with ultrasonication, dried with compressed nitrogen flow, and treated with plasma for 15 min. 50 μL NiO_x solution was dropped onto the FTO substrates and spinned at 4000 rpm for 30 s. Annealing was then applied at 150 °C in air for 20 min before these substrates were quickly transferred into a N_2-filled glovebox. The SAM layer was deposited on NiO_x surface at 4000 rpm for 30 s and annealing at 100 °C for 10 min. The perovskite layer was prepared by spin-coating with a program of 1000 rpm for 10 s then 4000 rpm for 40 s, followed by annealing in air at 210 °C for 5 min. For surface treatment, the $Yb(TFSI)_3$ or NaTFSI solutions on perovskite layers were spin-coated at 4000 rpm for 30 s and then post-annealed in a N_2-filled glove box at 65 °C for 10 min. The PCBM layer was deposited at 2000 rpm for 30 s and the BCP layer was deposited on PCBM surface at 4000 rpm for 30 s. Finally, 90 nm thick silver electrode was thermally evaporated on top of BCP.

Film characterizations:

The X-ray photoelectron spectroscopy (XPS) spectra, in-depth analysis XPS (Eching Ion: Ar^+, Ion Enerhy: 2 keV, Raster Size:1.75 mm, Etch Cycle:300 s) spectra and the ultraviolet photoelectron spectroscopy (UPS) spectra were collected on monochromatized Al K-alpha targets using an X-ray photoelectron spectrometer (Escalab Xi+) manufactured by Thermo Fisher Scientific. The Fourier-transform infrared (FTIR) spectra were collected using a Fourier transform infrared spectrometer (VERTEX 70, Brooke, Germany). The surface morphology of perovskite films and device cross-sectional images were obtained by field emission scanning electron microscopy (SEM, HATACHI, SU-8020). The distribution of elements was obtained by X-ray energy spectroscopy (EDS, Hitachi SU-8020). The atomic force microscope (AFM) and Kelvin probe microscopy (KPFM) images were obtained using a four-probe setup (Dimension Icon, BRUKER). The steady-state photoluminescence (PL) and the time-resolved photoluminescence (TRPL, excitation at 510 nm) were measured by time-resolved spectroscopy (PicoQuant 300, PICOQUANT). The ultraviolet visible (UV–vis) absorption spectra were obtained using a UV-visible spectrophotometer (UV-3600, Shimadzu). The X-ray diffraction (XRD) and grazing incidence XRD (GIXRD) were obtained by high resolution X-ray diffractometer (SmartLab, JEOL Japan Electronics Co., Ltd). Ambient stability test of perovskite films was performed at a RH of 20-25%.

Device characterizations:

The *J-V* characteristics of PSCs were performed at 100 mW cm^{-2} illumination using a solar simulator (SS-F5-3A, Enlitech) calibrated with an NREL-traceable KG5-filtered silicon reference cell for light intensity calibration and the device area was defined by a metal mask with an aperture area of 0.09 cm^2. The external quantum efficiency (EQE) of the device was measured using a QTest Station 500TI system (ESB-6, Enlitech Technology Co. Ltd). The QTest Station 2000 ADI system (Crowntech, Inc.) was used to record the stabilized power output (SPO) of devices. Space charge limiting currents (SCLC) were measured in dark with devices of FTO/NiO_x/perovskite/spiro-OMeTAD/Au. The capacitance voltage (*C-V*) characteristics of devices were measured on a Zahner Zennium electrochemical workstation (AMETEK-Modulab XM, USA). The *C-V* data were collected on a Zahner Zennium electrochemical workstation (AMETEK-Modulab XM, USA). *J-V*

curves at different light levels were obtained to determine the correlation between V_{OC} and light intensity. The dark state *J-V* characteristics were obtained by measuring the *J-V* curve of the device in dark environment. The ion migration activation energy was evaluated on a temperature-dependent vaccum probe setup (CGO-4, Cindbest, China), with the device structure of FTO/perovskite/(with or without Yb^{3+})/Au. The device ambient stability was tested by storing devices in an environment with RH of 20-25%. Thermal stability was conducted by continuous heating devices at 65 °C for 350 h in a nitrogen (N_2)-filled glove box. The operational stability was performed under continuous tracking at the maximum power point (MPP) using a 1-sun equivalent white-light LED array (Constant bias voltage: 1.05 V, interval time: 2 h, Multi-Channels Solar Cells Stability Test System, Wuhan 91PVKSolar Technology Co. Ltd, China).

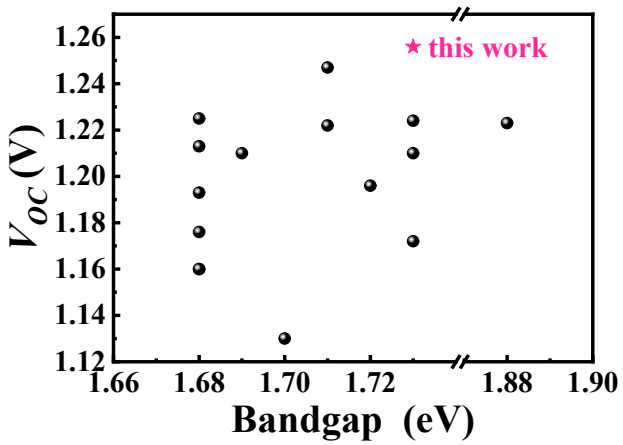

Fig. S1. Representative V_{OC}s of inverted structure inorganic PSCs collected from recent publications (ref.1-16, the detailed PV parameters are shown in **Table S1**).

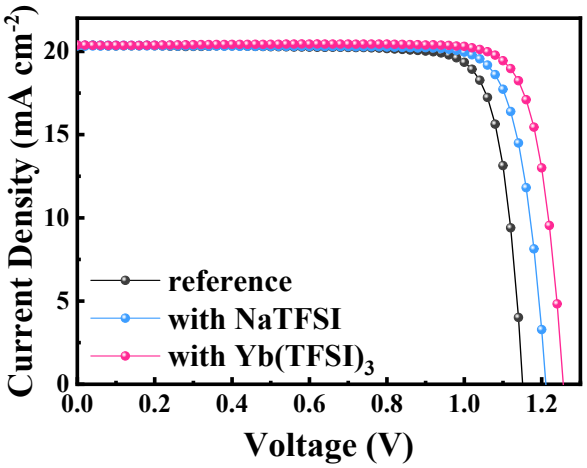

Fig. S2. *J-V* curves of inorganic PSCs without and with $Yb(TFSI)_3$ or NaTFSI surface treatment (under 100 mW cm^{-2} illumination, device active area is 0.09 cm^{-2}).

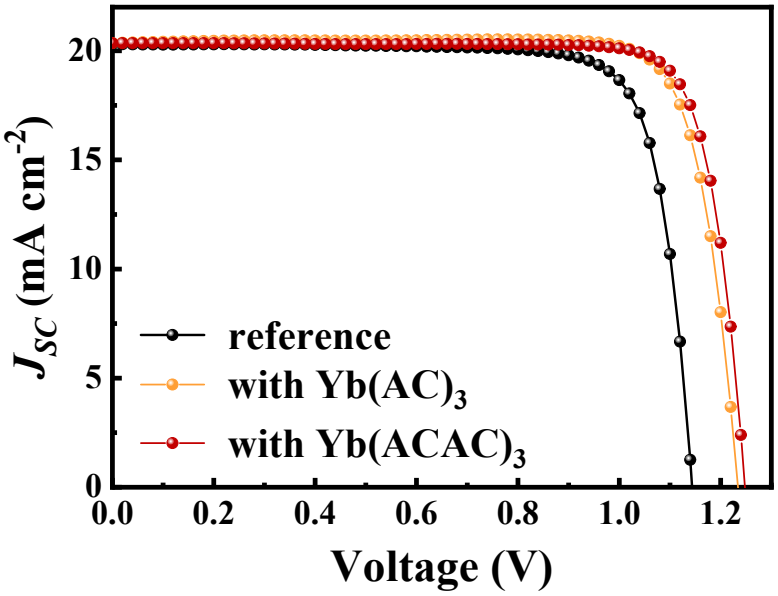

Fig. S3. *J-V* curves of PSCs without and with different Yb-salts treatment under 100 mW cm^{-2} illumination (the active area is 0.09 cm^{-2}).

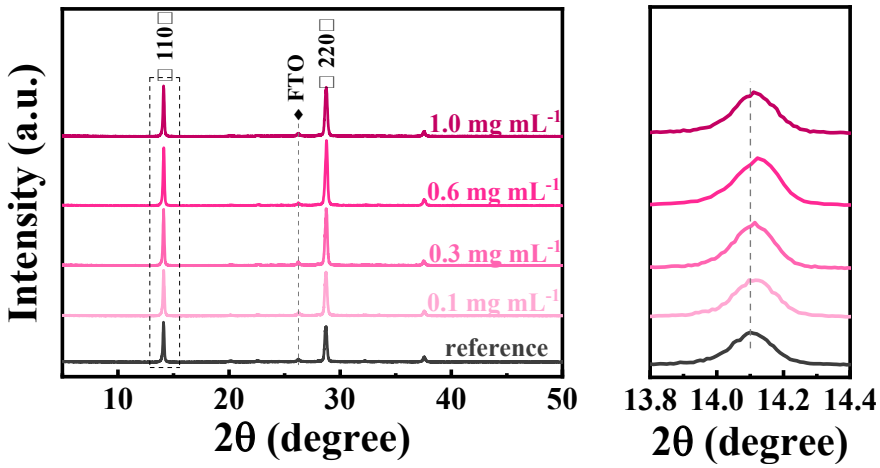

Fig. S4. XRD patterns of inorganic perovskite films with different amounts of Yb^{3+} treatment (inset: zoom-in (110) facet).

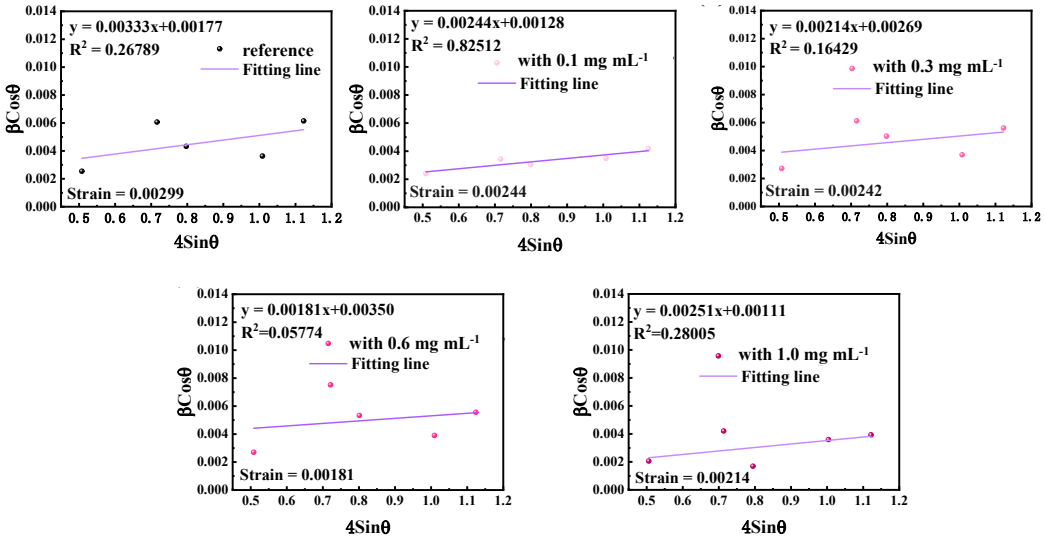

Fig. S5. Williamson-Hall analysis of perovskite films without and with different amounts of Yb^{3+} treatment.

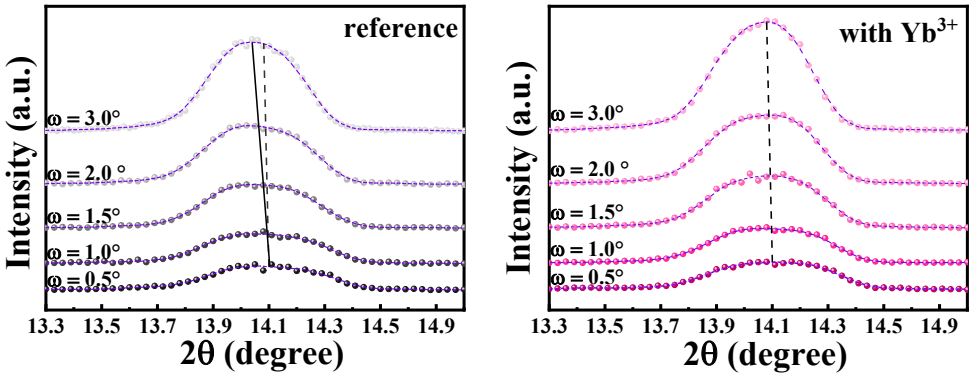

Fig. S6. GIXRD patterns of perovskite films without and with 0.3 mg mL^{-1} Yb^{3+} treatment.

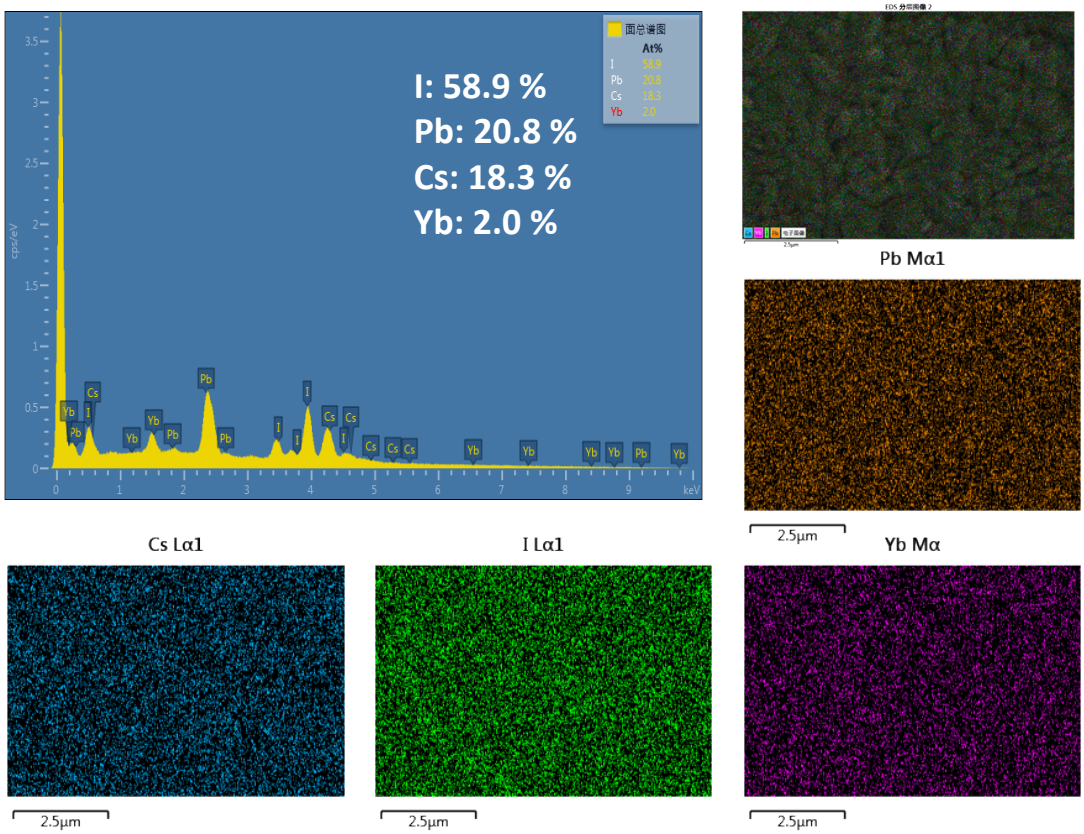

Fig. S7. EDS elemental mapping of inorganic perovskite film with Yb^{3+} surface treatment.

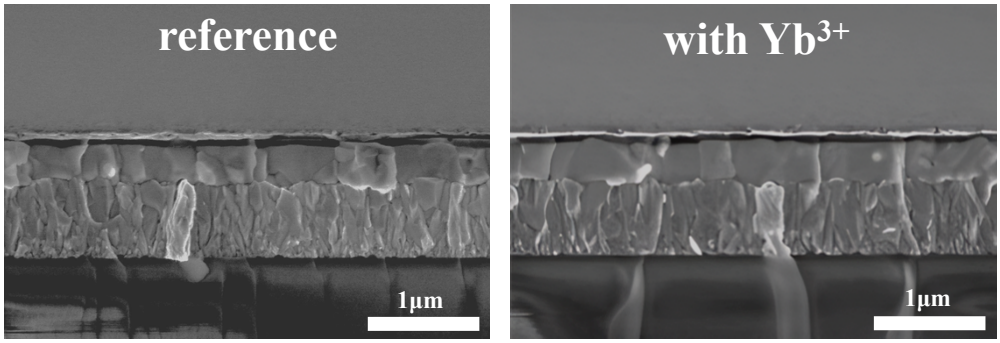

Fig. S8. Cross-sectional SEM images of inorganic PSCs without and with Yb^{3+} treatment.

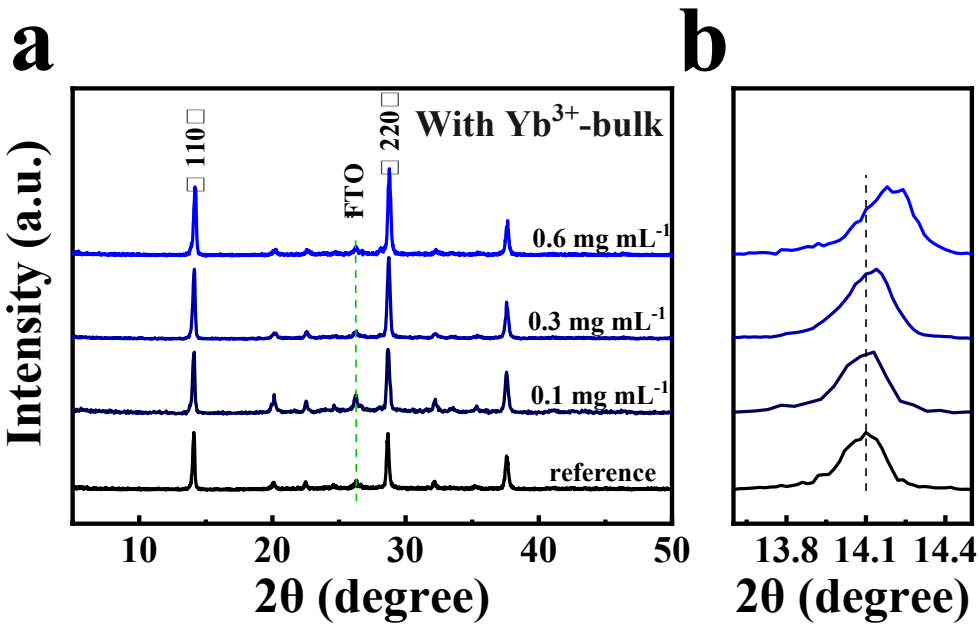

Fig. S9. XRD patterns of inorganic perovskite films (a) with different amounts of Yb^{3+}-bulk-incorporation (b) zoom-in (110) facet.

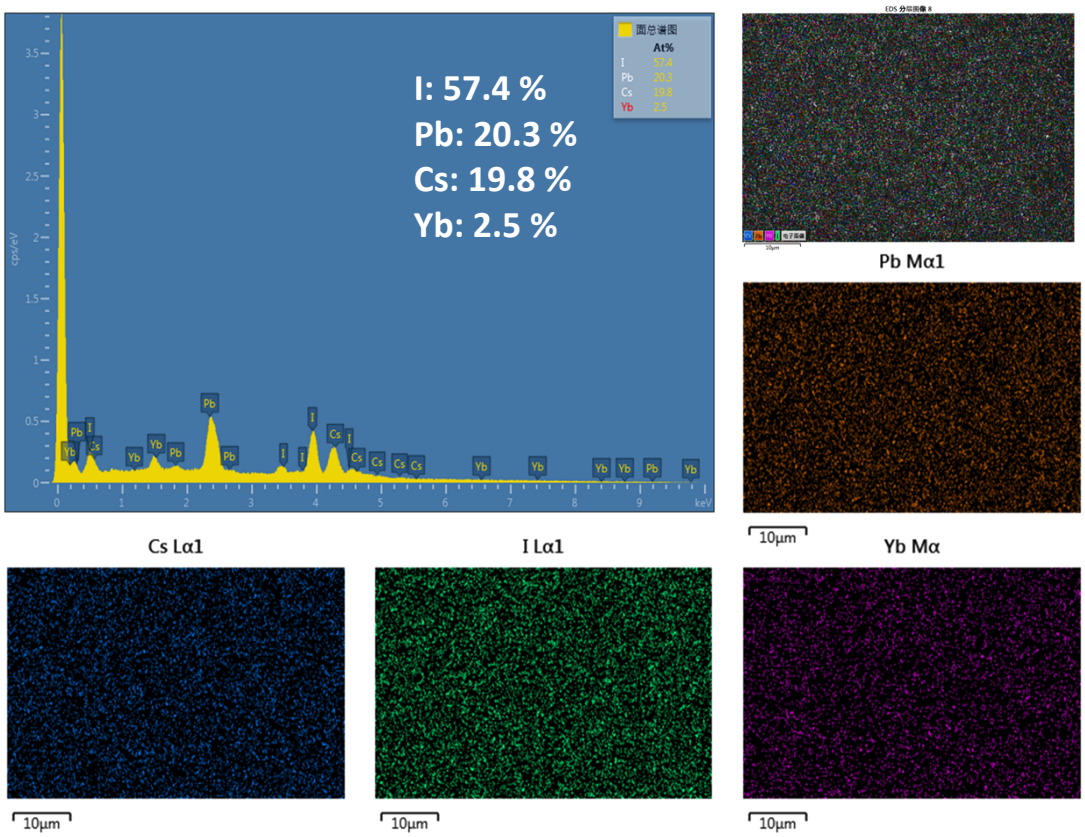

Fig. S10. EDS elemental mapping of inorganic perovskite film with 0.3 mg mL^{-1} Yb^{3+}-bulk.

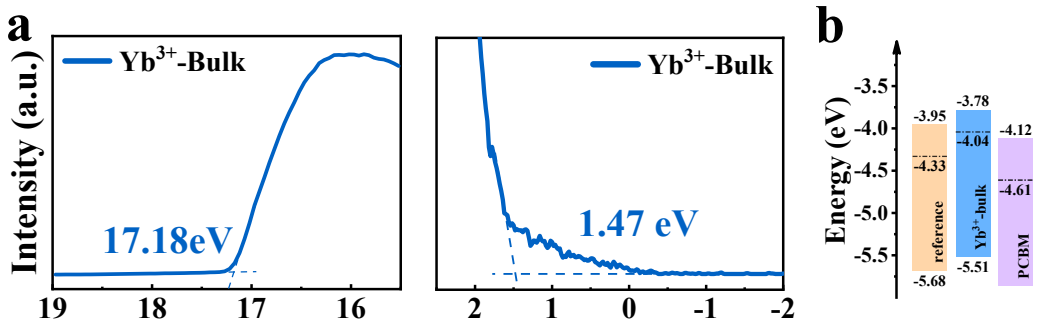

Fig. S11. (a) UPS spectra of Yb^{3+}-bulk incorporated perovskite thin film. (b) energy level diagram (values *vs* vacuum).

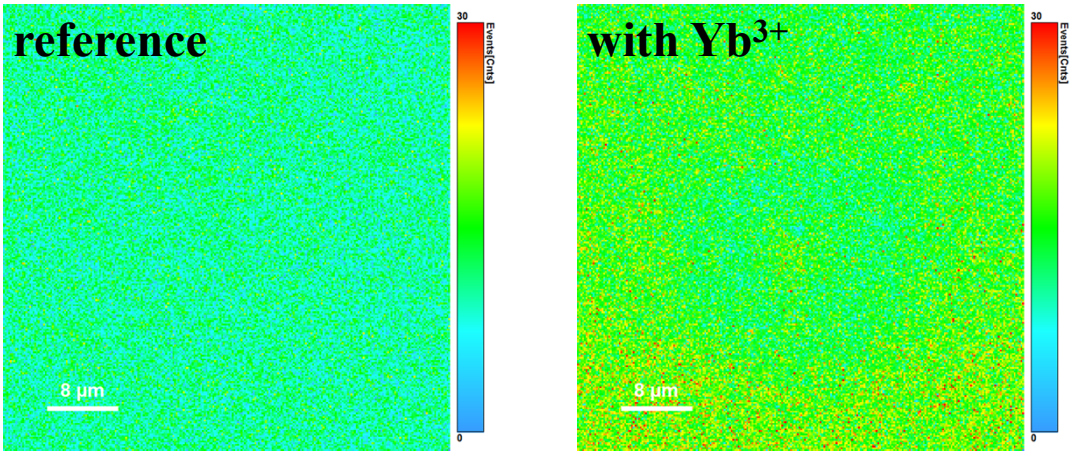

Fig. S12. PL-mapping images of inorganic perovskite thin films without and with Yb^{3+} treatment

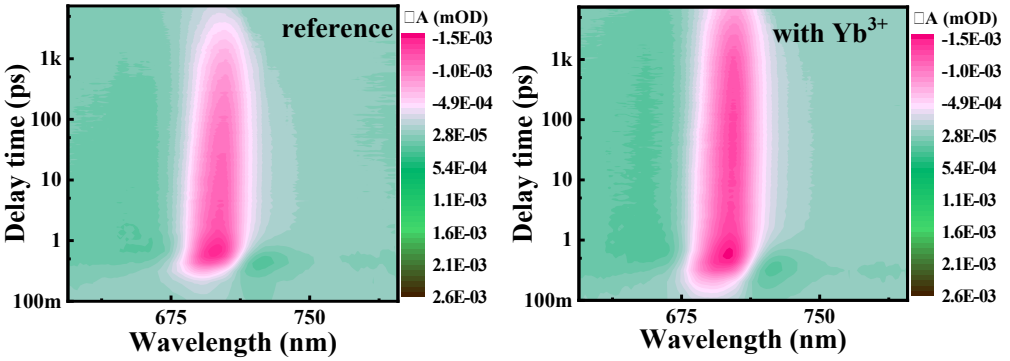

Fig. S13. The 2D contour plot of TAS of the photoinduced absorption as a function of wavelength and delay time for perovskite films without and with Yb^{3+} treatment.

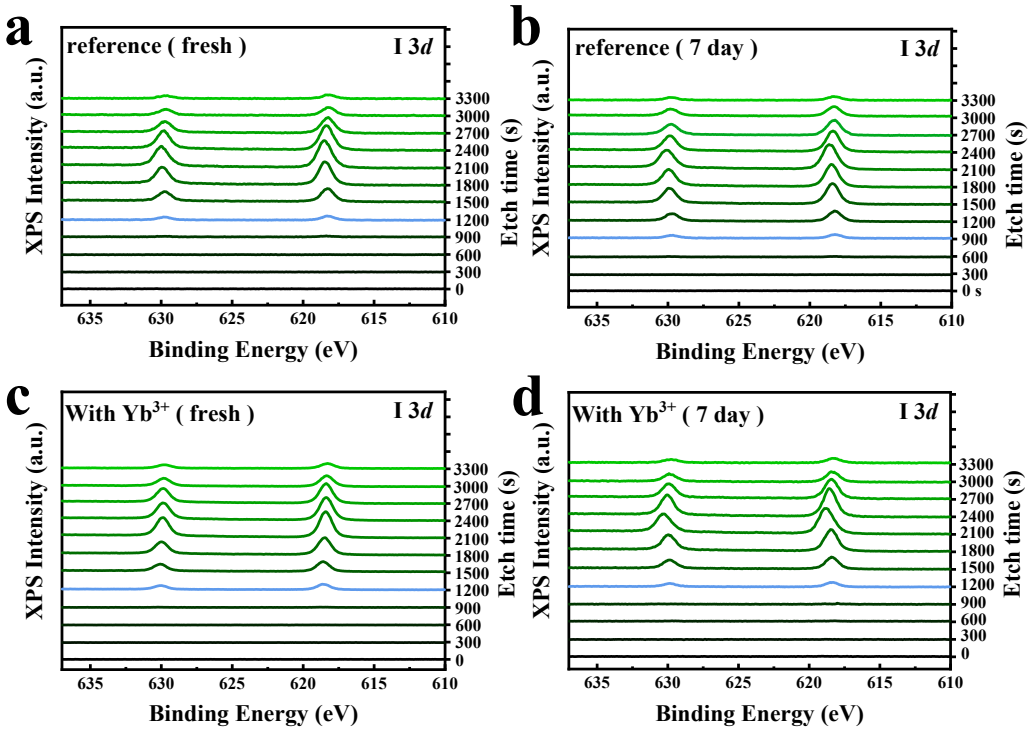

Fig. S14. XPS spectra of I 3*d* from perovskite films (a, b) without and (c, d) with $Yb(TFSI)_3$ treatment. (a, c) Fresh films and (b, d) films after 7 days of continuous exposure to one sun light. The stacked samples have the structure FTO/NiO_x/SAM/perovskite/(without or with Yb^{3+})/PCBM.

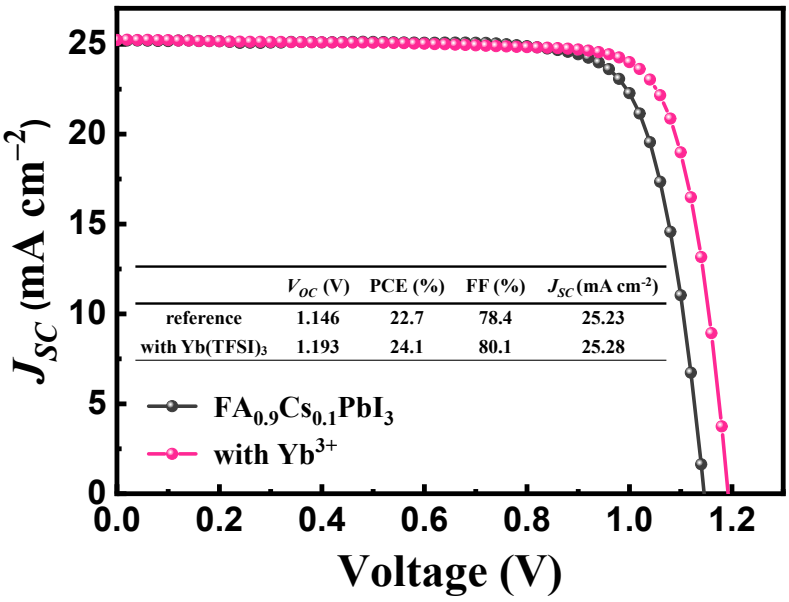

Fig. S15. *J-V* curves of $FA_{0.9}Cs_{0.1}PbI_3$ hybrid PSCs (n-i-p) without and with $Yb(TFSI)_3$ surface treatment (under 100 mW cm^{-2} illumination, device active area is 0.09 cm^{-2}). The device structure is FTO/SnO_2/ $FA_{0.9}Cs_{0.1}PbI_3$/with or without Yb^{3+}/Spiro-OMeTAD/Au.

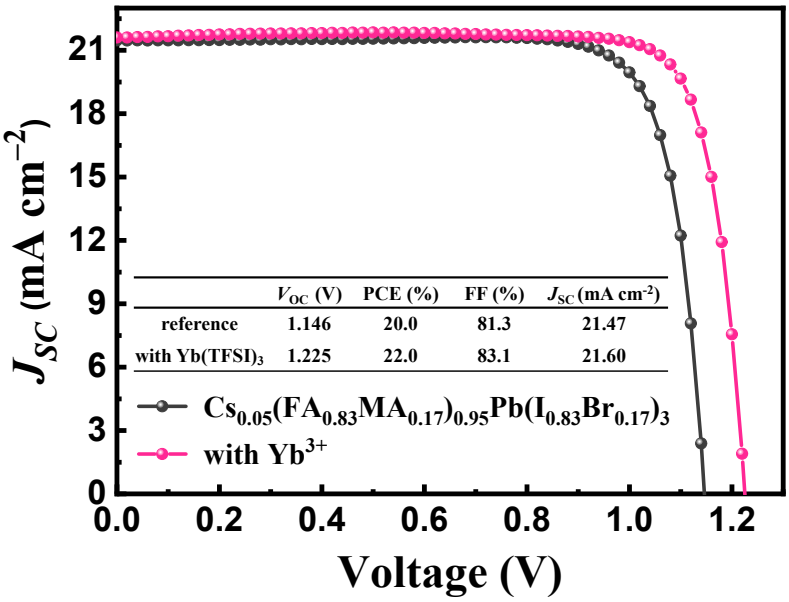

Fig. S16. *J-V* curves of $Cs_{0.05}(FA_{0.83}MA_{0.17})_{0.95}Pb(I_{0.83}Br_{0.17})_3$ hybrid PSCs (p-i-n) without and with $Yb(TFSI)_3$ surface treatment (under 100 mW cm^{-2} illumination, device active area is 0.09 cm^{-2}). The device structure is FTO/NiO_x/MeO-2PACz/ $Cs_{0.05}(FA_{0.83}MA_{0.17})_{0.95}Pb(I_{0.83}Br_{0.17})_3$/with or without Yb^{3+}/PCBM/BCP/Ag.

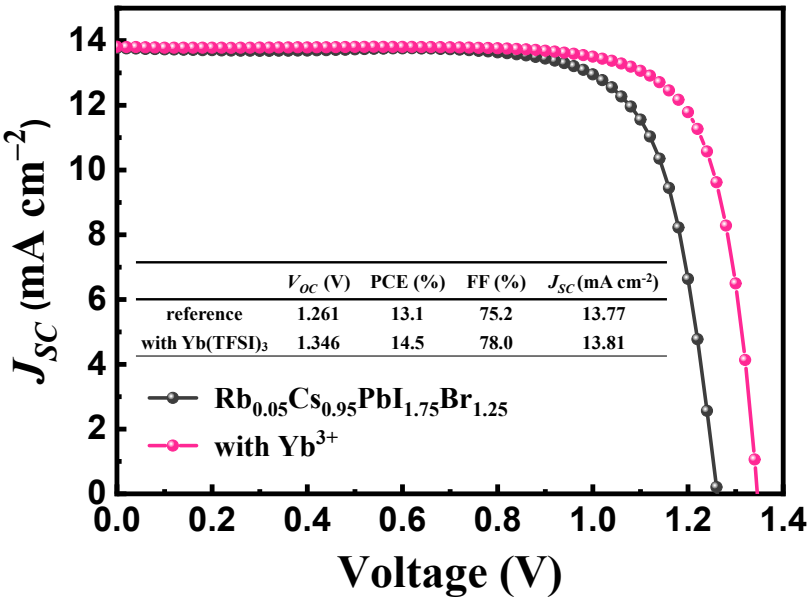

Fig. S17. *J-V* curves of $Rb_{0.05}Cs_{0.95}PbI_{1.75}Br_{1.25}$ inorganic PSCs (p-i-n) without and with $Yb(TFSI)_3$ surface treatment (under 100 mW cm^{-2} illumination, device active area is 0.09 cm^{-2}). The device structure is FTO/NiO_x/MeO-2PACz/$Rb_{0.05}Cs_{0.95}PbI_{1.75}Br_{1.25}$/with or without Yb^{3+}/PCBM/BCP/Ag.

Table S1. Summary of device structures and photovoltaic parameters of inverted inorganic PSCs.

Device structure	Eg (eV)	V_{OC} (V)	J_{SC} (mA cm^{-2})	FF (%)	PCE (%)	ref.
ITO/P3CT-N/$CsPbI_3$/PCBM/C_{60}/BCP/Ag	1.68	1.213	20.35	80.37	19.84	[1]
FTO/P3CT/$CsPbI_3$/PACl/PCBM/BCP/Ag	1.70	1.130	21.36	84.0	20.17	[2]
ITO/MeO-2PACz/β-$CsPbI_3$/α-$CsPbI_3$/PCBM/BCP/Ag	1.68	1.16	20.64	84.17	20.17	[3]
ITO/P3CT-N/$CsPbI_2Br$/PCBM/C_{60}/BCP/Ag	1.88	1.223	16.35	16.35	15.92	[4]
ITO/NiO_x/$CsPbI_xBr_{3-x}$/ZnO/C_{60}/Ag	1.78	1.16	17.7	78.60	16.1	[5]
ITO/PTAA/OMXene-$CsPbI_3$/CPTA/BCP/Ag	1.69	1.21	19.86	81.96	19.69	[6]
FTO/NiO_x/ $CsPbI_xBr_{3-x}$/PCBM/BCP/Ag	1.73	1.21	20.33	83.6	20.6	[7]
ITO/NiO_x/$CsPbI_{2.85}Br_{0.15}$/PCBM/BCP/Ag	1.71	1.222	19.92	83.67	20.38	[8]
ITO/P3CT-N/$CsPbI_3$/PCBM/C_{60}/BCP/Ag	1.68	1.225	20.33	77.37	19.27	[9]
ITO/NiO_x/$CsPbI_{2.85}Br_{0.15}$/PCBM/BCP/Cu	1.72	1.196	19.30	83.79	19.34	[10]
ITO/P3CT-N/$CsPbI_3$/PCBM/C_{60}/BCP/Ag	1.68	1.160	20.46	81.13	19.25	[11]
ITO/P3CT-N/$CsPbI_3$/PCBM/C_{60}/TPBi/Cu	1.73	1.172	20.58	78.84	19.01	[12]
ITO/P3CT-N/$CsPbI_3$/PCBM/C_{60}/BCP/Ag	1.68	1.176	20.10	80.04	18.93	[13]
ITO/MeO-2PACz/P3CT-N/$CsPbI_3$/PCBM/C_{60}/TPBi/Ag	1.68	1.193	20.68	81.95	20.22	[14]
FTO/NiO_x/MeO-2PACz/$CsPbIxBr_{3-x}$ /PCBM/BCP/Ag	1.73	1.224	20.36	84.2	21.0	[15]
ITO/NiO_x/P3CT-N/$CsPbI_{2.85}Br_{0.15}$ /PCBM/BCP/Ag	1.71	1.247	19.62	84.97	20.80	[16]
ITO/NiO_x/MeO-2PACz/$CsPbIxBr_{3-x}$ /PCBM/BCP/Ag	1.73	1.256	20.38	83.6	21.4	This work

Note: Indium-Tin Oxide (ITO) glass; F-doped tin oxide (FTO) glass; Poly[3-(4-carboxylatebutyl)thiophene]–CH_3NH_2 (P3CT-N); Poly[3-(4-carboxylatebutyl)thiophene] (P3CT, Mw: 30-40k); [2-(3,6-Dimethoxy-9H-carbazol-9-yl)ethyl]phosphonic acid (MeO-2PACz); Fullerene C_{60} (C_{60}); Poly(triaryl amine) (PTAA); propylamine hydrochloride (PACl); 1,3,5-tris(1-phenyl-1H-benzimidazol-2-yl)benzene (TPBi); [6,6]-phenyl-C61-butyric acid methyl ester ($PC_{61}BM$); bathocuproine (BCP).

Table S2. Hysteresis of the reference and different amount of Yb^{3+}-treated inorganic PSCs. Devices with an active area of 0.09 cm^2 were illuminated under 1 sun irradiation.

Device	V_{OC} (V)	PCE (%)	FF (%)	J_{SC} (mA cm^{-2})
reference-RS	1.151	19.3	82.5	20.37
reference-FS	1.100	18.2	81.6	20.20
Yb^{3+}-RS	1.256	21.4	83.6	20.38
Yb^{3+}-FS	1.241	21.0	83.1	20.37

Table S3. *J-V* parameters of the reference and NaTFSI or $Yb(TFSI)_3$ treatment inorganic PSCs. Devices with an active area of 0.09 cm^2 were illuminated under 1 sun irradiation.

Device	V_{OC} **(V)**	**PCE (%)**	**FF (%)**	J_{SC} **(mA** cm^{-2}**)**
reference	1.151	19.3	82.5	20.37
with NaTFSI	1.211	20.3	82.5	20.37
with $Yb(TFSI)_3$	1.256	21.4	83.6	20.38

Table S4. The *J-V* parameters of the reference and with different Yb salts-treated inorganic PSCs. These devices were evaluated under 100 mW cm^{-2} (AM1.5 G) illumination with an active area of 0.09 cm^2.

Device	V_{OC} (V)	PCE (%)	FF (%)	J_{SC} (mA cm^{-2})
reference	1.144	18.7	80.4	20.31
with $Yb(AO)_3$	1.234	20.8	82.7	20.35
with $Yb(ACAC)_3$	1.248	21.1	82.9	20.35

Table S5. Charge lifetimes in perovskite films with and without Yb^{3+} treatment from TRPL measurement.

	τ_{ave} (ns)	τ_1 (ns)	Amplitude τ_1 (%)	τ_2 (ns)	Amplitude τ_2 (%)
reference	54.84	123.28	19.68	38.90	80.32
with Yb^{3+}	109.56	160.90	51.37	83.46	48.63

References

1. S. Fu, J. Le, X. Guo, N. Sun, W. Zhang, W. Song and J. Fang, *Advanced Materials*, 2022, **34**, 2205066.
2. S. Wang, M.-H. Li, Y. Zhang, Y. Jiang, L. Xu, F. Wang and J.-S. Hu, *Energy & Environmental Science*, 2023, **16**, 2572-2578.
3. R. Ji, Z. Zhang, Y. J. Hofstetter, R. Buschbeck, C. Hänisch, F. Paulus and Y. Vaynzof, *Nature Energy*, 2022, **7**, 1170-1179.
4. S. Fu, X. Li, L. Wan, W. Zhang, W. Song and J. Fang, *Nano-Micro Letters*, 2020, **12**, 170.
5. J. Wang, J. Zhang, Y. Zhou, H. Liu, Q. Xue, X. Li, C.-C. Chueh, H.-L. Yip, Z. Zhu and A. K. Y. Jen, *Nature Communications*, 2020, **11**, 177.
6. J. H. Heo, F. Zhang, J. K. Park, H. Joon Lee, D. S. Lee, S. J. Heo, J. M. Luther, J. J. Berry, K. Zhu and S. H. Im, *Joule*, 2022, **6**, 1672-1688.
7. T. Xu, W. Xiang, J. Yang, D. J. Kubicki, W. Tress, T. Chen, Z. Fang, Y. Liu and S. Liu, *Advanced Materials*, 2023, **35**, 2303346.
8. S. Wang, P. Wang, B. Shi, C. Sun, H. Sun, S. Qi, Q. Huang, S. Xu, Y. Zhao and X. Zhang, *Advanced Materials*, 2023, **35**, 2300581.
9. S. Fu, N. Sun, J. Le, W. Zhang, R. Miao, W. Zhang, Y. Kuang, W. Song and J. Fang, *ACS Applied Materials & Interfaces*, 2022, **14**, 30937-30945.
10. H. Sun, S. Wang, S. Qi, P. Wang, R. Li, B. Shi, Q. Zhang, Q. Huang, S. Xu, Y. Zhao and X. Zhang, *Advanced Functional Materials*, 2023, **33**, 2213913.
11. S. Fu, X. Li, J. Wan, W. Zhang, W. Song and J. Fang, *Advanced Functional Materials*, 2022, **32**, 2111116.
12. C. Lu, X. Li, X. Guo, S. Fu, W. Zhang, H. Yuan and J. Fang, *Chemical Engineering Journal*, 2023, **452**, 139495.
13. S. Fu, W. Zhang, X. Li, J. Guan, W. Song and J. Fang, *ACS Energy Letters*, 2021, **6**, 3661-3668.
14. C. Lu, X. Li, H. Yuan, W. Zhang, X. Guo, A. Liu, H. Yang, W. Li, Z. Cui, Y. Hu and J. Fang, *Chemical Engineering Journal*, 2024, **480**, 147267.
15. T. Xu, W. Xiang, X. Ru, Z. Wang, Y. Liu, N. Li, H. Xu and S. Liu, *Advanced Materials*, **n/a**, 2312237.
16. S. Wang, S. Qi, H. Sun, P. Wang, Y. Zhao and X. Zhang, *Angewandte Chemie International Edition*, 2024, **63**, e202400018.